

# Hardware Implementation of Fano Decoder for PAC Codes

Amir Mozammel<sup>1</sup>, *Student Member, IEEE*

**Abstract**—This paper proposes a hardware implementation architecture for Fano decoding of polarization-adjusted convolutional (PAC) codes. This architecture maintains a trade-off between the error-correction performance and throughput of the decoder by implementing tree search constraining methods. The performance of the proposed decoder is evaluated on FPGA and ASIC using Xilinx Nexys 4 Artix<sup>®</sup>-7 and TSMC 28 nm 0.72 V library, respectively. The PAC decoder can be clocked at 400 MHz and reach an average information throughput of 15.10 Mb/s at 3.5 dB signal-to-noise ratio for a block length of 128 and code rate of 1/2.

**Index Terms**—PAC codes, sequential decoding, Fano, polar codes, VLSI.

## I. INTRODUCTION

**P**OLARIZATION-adjusted convolutional (PAC) codes are a new class of error-correcting codes that have been shown to achieve near-optimum performance [1]. By combining ideas from channel polarization [2] and convolutional coding [3], PAC codes create an overall encoding transform that achieves a performance near the information-theoretic limits at short block lengths.

Polar codes provably achieve the symmetric channel capacity of any given discrete memoryless channel. The basic algorithm for decoding polar codes is the successive cancellation (SC) decoding [2]. Various architectures for hardware implementation of SC decoding algorithm have been reported in the literature [4]–[11]. Many of the proposed implementations employ unrolling and pipelining techniques to improve the throughput of SC decoder. Due to its sub-optimality, SC decoder suffers from poor error-correction performance for short and moderate block lengths. To improve the performance of SC decoder, SC list decoding (SCL) has been proposed [12]. The error-correction performance of SCL decoder can be improved further by concatenating polar codes with a Cyclic Redundancy Check (CRC). There are some high-throughput SCL and SCL-CRC decoder implementations in the literature [11], [13], [14]. To achieve a high-throughput, the Belief Propagation (BP) algorithm has also been implemented for decoding polar codes [15].

The optimal algorithms for decoding convolutional codes are Viterbi [16], and BCJR algorithms [17], which are maximum likelihood and maximum a posteriori (MAP) decoders, respectively. For practical implementations, especially when the constraint length is large, sub-optimal decoding algorithms are also of interest. Two well-known sub-optimal decoding algorithms are sequential decoding [18], and majority-logic

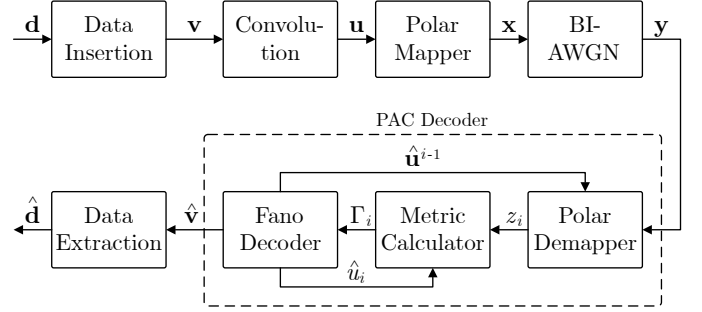


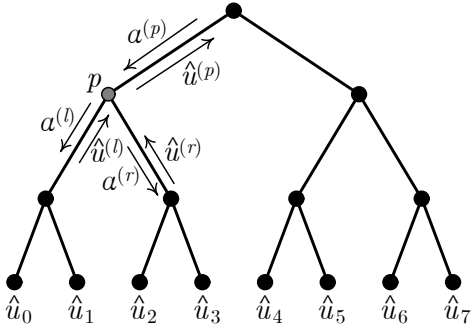
Fig. 1. PAC coding scheme.

or threshold decoding [19]. Fano algorithm [20] and Stack algorithm [21], [22] are the two commonly used sequential decoding algorithms. Because of the larger memory and sorting operation required for the Stack algorithm, the Fano algorithm is more favorable for practical hardware implementation, especially when the constraint length is large. To improve the throughput of the Fano decoder, bidirectional and parallel decoding techniques have been used [23]–[25]. Several hardware implementations of sequential decoders have been reported in the literature. A reconfigurable hardware architecture for Fano decoding has been proposed in [26]. Hardware implementations of sequential decoding algorithm have been used in deep-space communication [27], [28] and satellite communication [29]. Sequential decoding algorithm has also been used for decoding polar codes in [30].

Simulation results of [1] show that under sequential decoding, PAC codes can achieve the dispersion approximation (the finite-length capacity approximation) [31]. For some code rates and block length of 128, simulation results show that PAC codes under Fano decoding outperform 5G standard polar codes [32]. An efficient list decoding algorithm for PAC codes has been introduced in [33]. It has been shown that using a list size of 128, list decoding of PAC codes can achieve the same performance as sequential decoding of [1]. A performance and complexity comparison of sequential decoding and list decoding of PAC codes has been performed in [34]. To the best of the author's knowledge, decoding of PAC codes has never been implemented in hardware. The goal of the present paper is to discuss the hardware implementation of Fano decoding for PAC codes.

Throughout this paper, all vectors are over the binary field  $\text{GF}(2)$ . We denote vectors by boldface letters. Unless otherwise noted, all logarithmic functions  $\log$  are in base 2. For any set  $\mathcal{A} \subseteq \{0, 2, \dots, N - 1\}$ , we denote its complement by  $\mathcal{A}^c = \{i : i \notin \mathcal{A}\}$ . For any vector  $\mathbf{y}$  and set  $\mathcal{A}$ ,  $\mathbf{y}_{\mathcal{A}}$  denotes the sub-

The author is with the Department of Electrical-Electronics Engineering, Bilkent University, Ankara TR-06800, Turkey (e-mail: a.mozammel@ee.bilkent.edu.tr).

Fig. 2. SC decoder tree for  $N = 8$ .

vector  $(y_i : i \in \mathcal{A})$ . For any vector  $\mathbf{y}$ ,  $\mathbf{y}^j = (y_0, y_2, \dots, y_j)$ . We define a sign function  $\text{sgn}(l)$  such that

$$\text{sgn}(l) := \begin{cases} +1, & \text{if } l \geq 0, \\ -1, & \text{otherwise.} \end{cases}$$

The rest of this paper is organized as follows. Section II gives a brief discussion of polar codes, convolutional codes, and PAC codes and explains their decoding algorithms. Section III discusses two early termination techniques for reducing the search complexity of the Fano decoder. In Section IV we provide a simplified path metric and introduce a hardware architecture for Fano decoding of PAC codes. Implementation results of the proposed PAC Fano decoder are presented and compared with the state-of-the-art polar decoders in Section V. Section VI concludes the paper and provides suggestions for future work.

## II. PRELIMINARIES

PAC coding scheme combines convolution and polar transform. For this reason, in this section, we provide a brief introduction to convolutional codes and polar codes. Later, we will introduce PAC coding scheme and the related terminologies needed to better understand the hardware architecture.

### A. Polar codes

1) *Encoding*: A polar code is specified by three parameters  $(N, K, \mathcal{A})$ , where  $N$  is the codeword length,  $K$  is the data length, and  $\mathcal{A}$  is the set of data (non-frozen) indices. These codes utilize the channel polarization that takes  $N$  independent copies of a given binary-input discrete memoryless channel (B-DMC)  $W$  and create a second set of  $N$  bit-channels  $\{W_i : 1 \leq i \leq N\}$  that shows a polarization effect. Asymptotically, a  $C(W)$  fraction of the bit-channel capacities  $I(W_i)$  approach 1, and the rest approach 0, where  $C(W)$  is the capacity of B-DMC. Before encoding, the data  $\mathbf{d}$  of length  $K$  is inserted into a data carrier word  $\mathbf{u}$  of length  $N$  in accordance with the set  $\mathcal{A}$  such that frozen indices  $(\mathbf{u}_{\mathcal{A}^c})$  are set to 0, and the data bits are assigned to non-frozen indices  $(\mathbf{u}_{\mathcal{A}})$ . The encoding of a polar code can be expressed by  $\mathbf{x} = \mathbf{u}\mathbf{F}^{\otimes n}$ , where  $\mathbf{u}$  and  $\mathbf{x}$  are the input and output of the encoder, respectively, and the generator matrix  $\mathbf{F}^{\otimes n}$  is the  $n$ -th Kronecker product of the kernel matrix  $\mathbf{F} = \begin{bmatrix} 1 & 0 \\ 1 & 1 \end{bmatrix}$ .

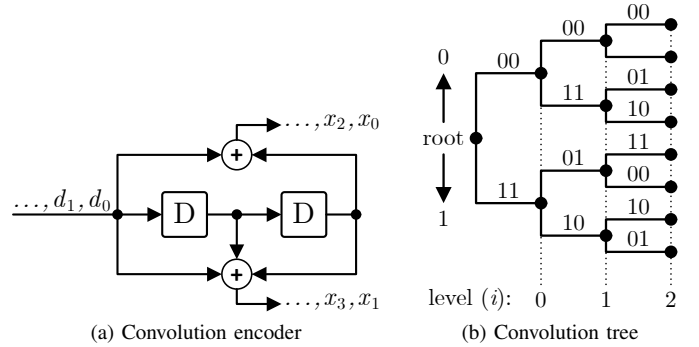


Fig. 3. Example of convolutional code.

2) *SC Decoding*: SC decoder of polar codes is a depth-first tree traversal algorithm with priority on the left branch. Fig. 2 shows a SC decoder tree for a polar code of length  $N = 8$ . The SC algorithm starts from the root of the tree at which the channel output log-likelihood ratios (LLRs)  $\alpha = (\alpha_0, \dots, \alpha_{N-1})$  are stored. For an AWGN channel with input  $\mathbf{x}$  and output  $\mathbf{y}$ , the channel output LLRs can be calculated using

$$\alpha_i = \ln \frac{P(y_i | x_i = 0)}{P(y_i | x_i = 1)} = \frac{2y_i}{\sigma^2}, \quad (1)$$

where  $\sigma^2$  is the noise variance of AWGN channel. Moving down the tree from a parent node  $p$  with LLRs  $\alpha^{(p)}$  of length  $N^{(p)}$ , the SC algorithm calculates the LLRs  $\alpha^{(l)}$  of the left child using the  $f$  function

$$\begin{aligned} \alpha_j^{(l)} &= f(\alpha_j^{(p)}, \alpha_{j+N^{(p)}/2}^{(p)}) \\ &= \text{sgn}(\alpha_j^{(p)})\text{sgn}(\alpha_{j+N^{(p)}/2}^{(p)}) \min(|\alpha_j^{(p)}|, |\alpha_{j+2^{s-1}}^{(p)}|), \quad (2) \end{aligned}$$

where  $0 \leq j \leq N^{(p)}/2 - 1$ . Once the SC algorithm reaches a leaf node, it generates the bit estimate  $\hat{u}_i$  using the leaf node LLR and  $\mathcal{A}$  such that if the node is non-frozen and the LLR is a negative value,  $\hat{u}_i = 1$ ; otherwise  $\hat{u}_i = 0$ . To calculate the LLR  $\alpha^{(r)}$  of the right child of node  $p$ , SC decoder uses the bit estimate vector  $\hat{\mathbf{u}}^{(l)}$  from left-hand-side sibling subtree and the  $g$  function

$$\alpha_j^{(r)} = g(\alpha_j^{(p)}, \alpha_{i+N^{(p)}/2}^{(p)}, \hat{u}_i^{(l)}) = \alpha_{i+N^{(p)}/2}^{(p)} + (1 - 2\hat{u}_i^{(l)})\alpha_j^{(p)}, \quad (3)$$

where  $0 \leq j \leq N^{(p)}/2 - 1$ . When the SC decoder goes up the tree, it combines the bit estimates by

$$\hat{u}_j^{(p)} = \begin{cases} \hat{u}_j^{(l)} \oplus \hat{u}_j^{(r)}, & \text{if } j < N^{(p)}/2, \\ \hat{u}_{j-N^{(p)}/2}^{(r)}, & \text{otherwise,} \end{cases} \quad (4)$$

for  $0 \leq j \leq N^{(p)}/2 - 1$ .

### B. Convolutional Codes

1) *Encoding*: Convolutional codes are a class of linear codes with a particular structure in the generator matrix so that the encoding operation can be viewed as a convolution operation. The encoding process of convolutional codes can be expressed by  $\mathbf{x} = \mathbf{d}\mathbf{G}$ , where  $\mathbf{d}$  and  $\mathbf{x}$  are the input and output

of the encoder, respectively, and  $\mathbf{G}$  is the generator matrix. For time-invariant convolutional codes,  $\mathbf{G}$  is a Toeplitz matrix in a row-reduced echelon form. In this case, the generator matrix is often characterized by a generator polynomial  $\mathbf{c} = (c_0, \dots, c_m)$ , where  $c_0 \neq 0$  and  $c_m \neq 0$ . The parameters  $m$  and  $m+1$  are called the memory order and constraint length of the convolution, respectively. A rate  $r_0 = k_0/n_0$  convolutional encoder with memory order  $m$  can be implemented as a  $k_0$ -input,  $n_0$ -output circuit with shift register of length  $m$ . Fig. 3a shows an example circuit for a convolutional code with  $k_0 = 1$ ,  $n_0 = 2$ ,  $m = 2$ ,  $\mathbf{c}_0 = (1, 0, 1)$ , and  $\mathbf{c}_1 = (1, 1, 1)$ , or  $\mathbf{c}_0 = 5$ , and  $\mathbf{c}_1 = 7$  in octal representation.

2) *Fano Decoding*: It is also possible to represent a convolutional code in the form of a tree through which each source word  $\mathbf{d} = (d_0, \dots, d_{K-1})$  of length  $K$  defines a path. Fig. 3b shows the first three levels of the tree corresponding to the convolutional code of Fig. 3a. For a node at level  $i$  of this tree, the upper-branch corresponds to  $d_i = 0$  and the lower-branch corresponds to  $d_i = 1$ . Each branch is labeled by the corresponding convolution output  $x_i$ . This representation turns the decoding problem into a tree search problem. For a received codeword, one of the paths through the code tree is correct and the others are incorrect. The Fano algorithm is a depth-first search algorithm that traverses through the code tree to find the correct path. If the search complexity (the total number of forward and backward moves) of the Fano decoder is not limited, it can achieve the capacity of any binary memoryless channel (BMC). However, the mean computation complexity increases unboundedly if the code rate  $R$  is larger than the cutoff rate  $R_0(W)$ . For  $R < R_0(W)$  it is possible to have reliable communication at a constant average computation complexity.

Fano algorithm uses a path metric  $\Gamma$  and a metric threshold  $T$  to identify the correct path. The function that the Fano decoder uses for calculating the path metric is called the Fano metric and is defined as

$$\Gamma_i = \sum_{j=0}^i \gamma_j = \sum_{j=0}^i \left[ \log_2 \frac{P(y_j|x_j)}{P(y_j)} - b_j \right], \quad (5)$$

where  $\gamma_j$  is the branch metric,  $P(y_j|x_j)$  is the channel transition probability,  $P(y_j)$  is the channel output probability, and  $b_j$  is a constant bias. Fano metric is the optimum metric for comparing paths of different lengths [35]. If the Fano metric grows along a given path, the algorithm considers it as a correct path and continues to search further along it. But if the metric drops significantly, the algorithm backtracks and searches other paths. This is accomplished by comparing the path metric with a threshold  $T$  in a way that whenever the path metric grows significantly on a forward search, the threshold is tightened (raised by threshold spacing  $\Delta$ ), and whenever the algorithm backtracks, the threshold is relaxed (lowered by  $\Delta$ ). In this way, no node is ever searched twice with the same threshold [36, p 372-373].

To explain the Fano algorithm, we examine the flowchart of Fig. 4. At the beginning of decoding, the threshold  $T$  and a search pointer  $i$  are initialized to 0. In the look forward block, the algorithm computes both metrics of the two branches  $d_i =$

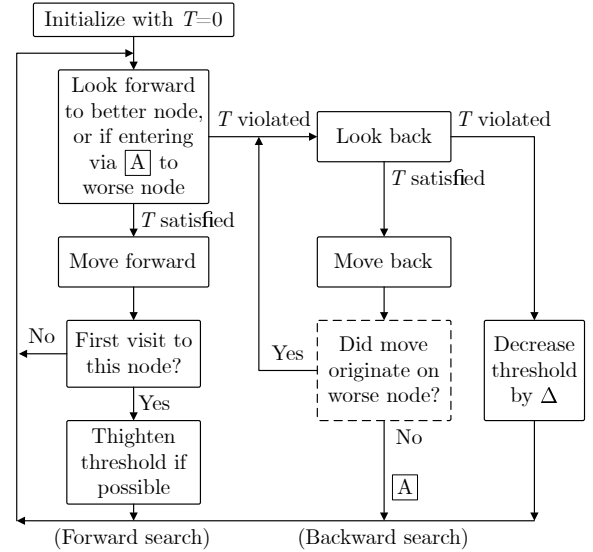


Fig. 4. Fano decoding algorithm for binary tree, reproduced from [36, p 373]

0 and  $d_i = 1$ , and if the algorithm is looking forward to better node, it adds the greater of the two branch metrics to the current path metric. If the look forward block is entered from  $[A]$ , it means that the better node has already been searched, the threshold  $T$  has been violated, and the algorithm must look to the worse node (the branch with the smaller branch metric). In either case, the Fano decoder compares the new path metric  $\Gamma_i$  with the threshold  $T$ , and if  $\Gamma_i \geq T$  ( $T$  satisfied), the algorithm moves forward by incrementing the search pointer  $i$ . After a forward move, if the node is visited for the first time, the threshold is tightened by increasing the threshold by integer multiples of  $\Delta$  such that the new threshold satisfies  $\Gamma_i - \Delta < T \leq \Gamma_i$ .

In the look forward block if  $\Gamma_i < T$  ( $T$  violated), the algorithm looks back and compares the previous path metric  $\Gamma_{i-1}$  with the threshold, and if  $\Gamma_{i-1} \geq T$  ( $T$  satisfied) it moves back by decrementing the search pointer  $i$ . If the backward move was made on the better of the two branches stemming from the node just reached (the better node), the worse node has to be searched next. But, if it was made on the worse branch, there is no branch left to be explored, and the algorithm must continue the backward search. If, during a backward look, the threshold  $T$  is violated, the algorithm cannot move back, and eventually, all paths from here have been searched and violated the current threshold. Thus, the algorithm decreases the threshold by  $\Delta$  and continues the forward search using the new threshold. The Fano algorithm keeps repeating these steps until it reaches the last level of the convolution tree, i.e.,  $i = N - 1$ , or a predefined termination criterion like maximum search limit is satisfied. An extensive study of the Fano decoder may be found in [37].

### C. PAC codes

1) *Encoding*: A PAC code is specified by four parameters  $(N, K, \mathcal{A}, \mathbf{c})$ , where  $N$  is the codeword length,  $K$  is the data length,  $\mathcal{A}$  is the data index set, and  $\mathbf{c}$  is the generator polynomial of convolution. The codeword length is constrained to be

a power of two,  $N = 2^n$  for  $n \geq 1$ , and data length  $K$  can be any integer between 1 and  $N$ . Fig. 1 shows the block diagram of the PAC coding scheme, which uses the Fano algorithm for decoding. The data insertion block receives a source word  $\mathbf{d}$  of length  $K$  and inserts it into a data carrier word  $\mathbf{v}$  of length  $N$  in accordance with the data index set  $\mathcal{A}$  such that  $\mathbf{v}_{\mathcal{A}} = \mathbf{d}$  and  $\mathbf{v}_{\mathcal{A}^c} = \mathbf{0}$ . Similar to polar codes, the bits that are fixed to zero are called frozen, whereas all the other bits are called non-frozen. The data carrier word  $\mathbf{v}$  goes through a convolution block, which is a rate one convolutional encoder with an impulse response  $\mathbf{c}$ . The resulting word  $\mathbf{u}$  goes through a polar mapper block, which is a rate one polar encoder. The overall encoding process of PAC codes can be expressed by  $\mathbf{x} = \mathbf{v}\mathbf{G}\mathbf{F}^{\otimes n}$ , where  $\mathbf{F}^{\otimes n}$  and  $\mathbf{G}$  are the generator matrices of polar codes and convolutional codes, respectively.

2) *Fano Decoding*: Fano decoding of PAC codes consists of three main blocks: polar demapper, metric calculator, and Fano decoder. Similar to the SC decoder of polar codes, the polar demapper operates on the polar tree of Fig. 2. But unlike the SC decoder, the polar demapper does not make any hard decision at the leaf-nodes of the polar tree, i.e., it does not generate any bit-estimate output  $\hat{u}_i$ . Rather, it receives the prior bit-estimates from the Fano decoder and passes the soft values of LLRs to the metric calculator block. In short, a polar demapper can be considered and implemented as a soft-in soft-out SC decoder. To distinguish the leaf nodes LLRs from the intermediate LLRs, we denote the leaf nodes LLRs by  $\mathbf{Z} = (z_0, \dots, z_{N-1})$ . The polar demapper receives the channel output LLRs  $\alpha$  that are calculated using (1) and based on the prior estimates of convolution output  $\hat{\mathbf{u}}^{i-1}$ , generates the leaf node LLRs  $\mathbf{Z}$ . Then the LLR  $z_i$  of  $i$ th leaf node is selected from  $\mathbf{Z}$ . Hence,  $z_i$  can be expressed by  $z_i = \frac{P(\mathbf{y}^N, \hat{\mathbf{u}}^{i-1} | \hat{u}_i = 0)}{P(\mathbf{y}^N, \hat{\mathbf{u}}^{i-1} | \hat{u}_i = 1)}$ .

A metric calculator block uses  $z_i$  to calculate the path metric  $\Gamma_i$  of node  $i$  based on the hypothesis  $\hat{u}_i = 0$  and  $\hat{u}_i = 1$ , which are also provided by the sequential decoder. Since the channel seen by the convolution operation of PAC codes is a channel with memory (polarized channel), the Fano metric of (5) is not suitable for Fano decoding of PAC codes. The path metric for PAC codes can be derived from (5) as

$$\Gamma_i = \log \frac{P(\mathbf{y}^N | \hat{\mathbf{u}}^i)}{P(\mathbf{y}^N)} - \sum_{j=0}^i b_j \quad (6)$$

and the path metric can be calculated using (6) as

$$\begin{aligned} \gamma_i(\hat{u}_i) &= \Gamma_i - \Gamma_{i-1} \\ &= \log \frac{P(\mathbf{y}^N | \hat{\mathbf{u}}^i)}{P(\mathbf{y}^N | \hat{\mathbf{u}}^{i-1})} - b_i \\ &= \log \frac{P(\mathbf{y}^N, \hat{\mathbf{u}}^{i-1} | \hat{u}_i)}{P(\mathbf{y}^N, \hat{\mathbf{u}}^{i-1})} - b_i. \end{aligned} \quad (7)$$

For a binary input channel with uniform input distribution, (7) can be reduced to

$$\gamma_i(\hat{u}_i) = 1 - \log(1 + e^{-(1-2\hat{u}_i)z_i}) - b_i, \quad (8)$$

where  $z_i$  is the output of polar demapper. For a detailed derivation of (7) and (8) we refer to [38]. Note that using the

branch metric  $\gamma_i(\hat{u}_i)$  we can easily calculate the path metric as  $\Gamma_i = \sum_{j=0}^i \gamma_j(\hat{u}_j)$ . A study on the metric function of PAC codes shows that using the bit-channel capacities  $I(W_i)$  as the bias value reduces the search complexity of PAC Fano decoder significantly [38]. For an AWGN channel, the bit-channel capacities  $I(W_i)$  can be calculated using methods like density evolution [39].

The Fano decoder of PAC codes uses  $\Gamma_i$  to identify the correct path in the convolution tree and consequently generates an estimate  $\hat{\mathbf{v}}$  of  $\mathbf{v}$ . The convolution tree of PAC codes is similar to the tree of Fig. 3b with a difference that for PAC codes, the convolution tree only branches at non-frozen nodes. The operation of PAC Fano decoder is also similar to the Fano decoder of conventional convolution codes shown in Fig. 4 with a single difference that upon a backward move, the PAC Fano decoder checks whether the currently reached node is frozen or non-frozen; if the node is frozen, there is no branch to be explored, and the algorithm must continue the backward search. This block is indicated with a dashed line in Fig. 4.

### III. CONSTRAINED TREE SEARCH

Depending on the severity of the noise, the Fano algorithm may fail to identify the correct path in the convolution tree and explore the wrong paths that may result in a frame error. In the following, we study two early termination criteria that stop the decoder whenever the Fano decoder is likely to make a frame error with high probability.

#### A. Number of Diversions from SC Path

A simulation in [34] shows that from 4000 decoding failures (decoding resulted in a frame error) of a PAC code of length  $N = 128$  and  $K = 64$  at  $E_b/N_0 = 2.5$  dB, in less than 1% of them, there are more than five bit-errors between the Fano decoder path and the SC path. Using this knowledge during a decoding session, we may terminate the decoding whenever the Fano path diversion from the SC path, DIV, exceeds a predefined number  $\text{DIV}_{\max}$ . Depending on the value of  $\text{DIV}_{\max}$ , this method reduces the search complexity of the Fano decoder at the cost of FER degradation.

#### B. Number of Moves

The search complexity of the Fano decoder is a random variable with a distribution that has heavy-tailed nature such that a small fraction of codewords require a very large search complexity [32]. For this reason, by limiting the total number of moves made by the Fano decoder during a single decoding session, we may introduce a small FER degradation, but we can reduce the search complexity of the decoder significantly. To accomplish this, while decoding a codeword, we count the number of Fano decoder moves  $\theta$  (backward and forward), and if it exceeds a limit  $\theta_{\max}$ , we terminate the decoding.

### IV. HARDWARE IMPLEMENTATION

In this section, first, we will introduce a simplified path metric function and examine the effect of quantization on the FER performance of PAC codes. We will then investigate the properties of three main blocks of a PAC Fano decoder from a hardware implementation perspective.

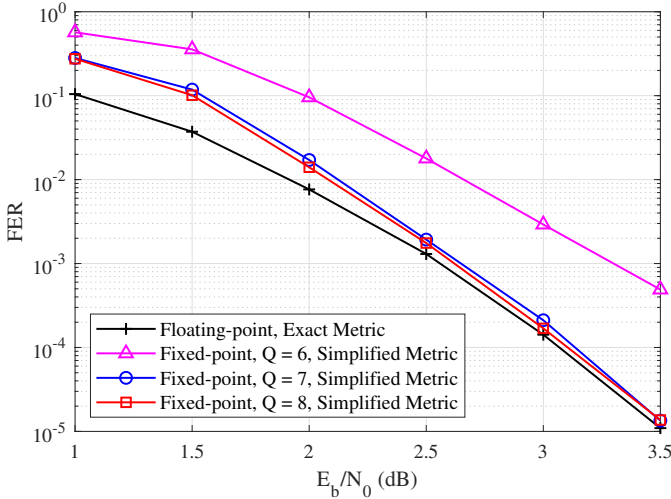


Fig. 5. FER performance of PAC Fano decoder using different quantization levels.

### A. Simplified Branch Metric and Quantization

The branch metric function of (8) is not a hardware-friendly function as it involves both logarithmic and exponential functions. The exact implementation of this function requires using a lookup table (LUT) to store the output value of it for the range of  $z_i$  and  $\hat{u}_i$ . The bias  $b_i$  value may be subtracted later.

To obtain a hardware friendly version of (8), we may adopt the approximation used for SCL decoding of polar codes [40]. This approximation uses  $\log(1 + e^{-(1-2\hat{u}_i)z_i}) \approx 0$  if  $\hat{u}_i = \frac{1}{2}(1 - \text{sgn}(z_i))$ , and  $\log(1 + e^{-(1-2\hat{u}_i)z_i}) \approx |z_i|$  otherwise. Using this approximation the branch metric reduces to

$$\gamma_i(\hat{u}_i) = \begin{cases} 1 - b_i, & \text{if } \hat{u}_i = \frac{1}{2}(1 - \text{sgn}(z_i)), \\ 1 - |z_i| - b_i, & \text{otherwise.} \end{cases} \quad (9)$$

Moreover, in our simulations (not presented here), we realized that using hard quantized (1-bit quantization) bit-channel capacities  $I(W_i)$  as the bias value does not degrade the FER performance of PAC Fano decoder.

Fig. 5 compares the FER performance of PAC Fano decoder using the exact path metric function (8) v. simplified path metric function (9). The channel LLRs are calculated according to (1) using a noise variance corresponding to  $E_b/N_0 = 3.5$  dB. Also shown in this figure is the effect of the number of quantization bits  $Q$  of LLRs on the decoder's FER performance. We represent the LLRs in the form of sign-magnitude using one, two, and  $Q-3$  bits for defining the sign, decimal part, and whole part of a number. Also, the floating-point decoder uses soft values of  $I(W_i)$ , whereas the fixed-point decoders use hard quantized values of  $I(W_i)$  as the bias.

In low SNR regime the approximation error is large since as SNR decreases the term  $\log(1 + e^{-(1-2\hat{u}_i)z_i})$  diverges from  $|z_i|$ . But as SNR increases, this error becomes negligible. Additionally, from this figure, we can conclude that the performance loss with 7-bit quantization is negligible.

### B. Architecture

1) *Polar Demapper*: A polar demapper can be implemented by modifying the SC decoder of polar codes as they both

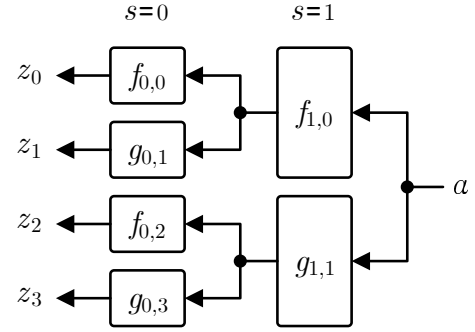


Fig. 6. Polar demapper for  $N = 4$ .

operate on the polar decoding tree of Fig. 2. In this regard, we adopt the fully parallel FFT-like architecture of [4] and apply the following modifications to make it operate as a polar demapper.

- 1) A polar demapper is required to generate the soft LLR values, so we remove the decision unit which was used to generate the bit-decisions at the leaf nodes of the SC decoding tree of Fig. 2.
- 2) The bit estimates  $\hat{u}$  are provided by the Fano decoder; hence we remove the bit estimates update unit and corresponding registers. Instead, we implement the bit estimates update function of (4) using a combinational circuit that receives the leaf node bit estimates from the Fano decoder and updates the intermediate bit estimates. The reason behind using a combinational circuit is to reduce the latency of polar demapper.
- 3) Due to the sequential nature of the Fano decoder, the  $z_i$  values are required to be generated in a natural order. We modify the bit-reversal architecture of [4] to generate the leaf node LLR values in a natural order.

Despite the similarity in architecture, the timing schedule of polar demapper is different from the one of SC decoder in the sense that the polar demapper generates the leaf-node LLR values  $z_i$  one at a time. Meaning that once it generated a leaf node LLR value, it remains idle until another leaf node LLR value is requested. Note that the next LLR value request may be for the immediate forward node or any other backward node. Hence, the polar demapper must be able to follow the Fano algorithm whenever it backtracks. To fulfill this requirement, we store all the intermediate LLR values until the end of each decoding session. By doing so, every time a new leaf node's LLR value is requested, the polar demapper does not have to start from the root of the SC decoding tree. Instead, it can start demapping from the least common ancestor of the current leaf node and the previous leaf node. The latter statement is only valid in the case of using a Fano decoder since it always moves from a current node either to its predecessor or to one of its immediate successors, and it never jumps.

Storing the intermediate LLR values requires  $N \log N$  memory elements. Compared to the line architecture proposed in [4] that uses  $N - 1$  memory for storing the intermediate LLR values, the polar demapper requires approximately  $\log N$  times larger memory. Moreover, the line architecture of [4] uses  $N/2$

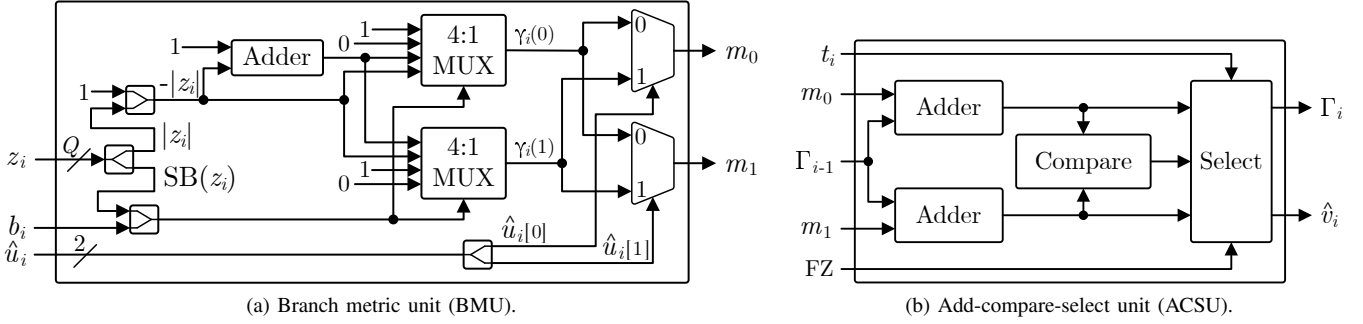


Fig. 7. Hardware diagram of the metric calculator block.

number of  $f$  blocks and  $N/2$  number of  $g$  blocks in total, whereas the FFT-like architecture implements same number of  $f$  and  $g$  blocks at each stage which results in  $\log N$  times larger area. The reason for using a fully parallel architecture for implementing the polar demapper is to avoid the routing (multiplexing) complexity and reduce the wire delay from the LLR register banks to the  $f$  and  $g$  blocks.

To understand the timing schedule of polar demapper, consider the polar demapper of Fig 6. To generate the LLR value  $z_i$  for the  $i$ th node the block  $X_{s,l}$  is activated, where  $X$  represents the type of operation (either  $f$  or  $g$ ),  $s$  is the stage which is determined by  $\text{ffs}^*(i)$  (find first set operation), and  $l$  is the ID number of the block determined by  $l = \frac{i}{2^s}$ . The  $\text{ffs}^*$  operation is defined as

$$\text{ffs}^*(i_{k-1} \dots i_1 i_0) = \begin{cases} \min(j) : i_j = 1, & \text{if } i > 0, \\ k - 1, & \text{if } i = 0, \end{cases} \quad (10)$$

where  $i_{k-1} \dots i_1 i_0$  is the binary representation of  $i$ . The control signals of blocks are connected in a way that once the output of a block is ready, it immediately activates its following block until reaching  $s = 0$ . Upon reaching  $s = 0$ , the polar demapper stops and waits for the next request.

TABLE I  
 $\gamma_i(\hat{u}_i)$  FOR DIFFERENT VALUES OF  $z_i$  AND  $b_i$ .

$\frac{1}{2}(1 - \text{sgn}(z_i))$	$b_i$	$\gamma_i(0)$	$\gamma_i(1)$
0	0	1	$1 -  z_i $
0	1	0	$- z_i $
1	0	$1 -  z_i $	1
1	1	$- z_i $	0

2) *Metric Calculator*: The task of the metric calculator block is to calculate and compare the path metrics for the two candidate nodes at level  $i$  of the convolution tree, which are currently being examined by the Fano decoder, and, depending on the Fano decoder's choice, output the best or worst path metric  $\Gamma_i$  along with the corresponding decision  $\hat{v}_i$ . A metric calculator block consists of two sub-blocks: branch metric unit (BMU) and add-compare-select unit (ACSU). The former calculates the branch metric  $\gamma_i(\hat{u}_i)$ , and the latter generates the path metric  $\Gamma_i$  and performs the compare and select operation.

Using the simplified branch metric function of (9) and assigning the hard quantized values of bit-channel capacities as the bias, we can tabulate  $\gamma_i(0)$  and  $\gamma_i(1)$  for all the possible values of  $b_i$  and  $\text{sgn}(z_i)$  in Table I. Since we represent the

LLRs in the form of sign-magnitude, the term  $\frac{1}{2}(1 - \text{sgn}(z_i))$  corresponds to the sign bit (SB) of  $z_i$ . Hence, we can simply implement this table using two 4-to-1 multiplexers (4:1 MUX) and one adder.

Fig. 7a shows the hardware diagram of the BMU sub-block. Once the demapping process is performed by the polar demapper, a multiplexer (MUX) selects  $z_i$  from the output of the polar demapper. This  $z_i$  is fed to the BMU sub-block along with the bias value  $b_i$ , and the convolution output estimates  $\hat{u}_i = (\hat{u}_{i,0}, \hat{u}_{i,1})$ , where  $\hat{u}_{i,0}$  and  $\hat{u}_{i,1}$  are the convolution output estimates for the two possible successor branches  $\hat{v}_i = 0$  and  $\hat{v}_i = 1$ , respectively. Two 4-to-1 multiplexers along with one adder generate the path metric  $\gamma_i(\hat{u}_i)$  for the two possible values of  $\hat{u}_i = 0$  and  $\hat{u}_i = 1$ . Finally, two 2-to-1 multiplexers select the proper values of  $\gamma_i$  in accordance with the values of  $\hat{u}_{i,0}$  and  $\hat{u}_{i,1}$ . Consequently, the  $m_0$  and  $m_1$  outputs of BMU sub-block correspond to the branch metric  $\gamma_i(\hat{u}_i)$  for the two hypotheses  $\hat{v}_i = 0$  and  $\hat{v}_i = 1$ , respectively.

The circuit diagram of ACSU is shown in Fig. 7b. The ACSU receives  $m_0$  and  $m_1$ , adds them to the previous path metric  $\Gamma_{i-1}$ , compares the resulting path metrics, and based on the value of an input  $t_i$ , either selects the best metric or the worst metric. The value of  $t_i$  is defined by the Fano decoder such that, when  $t_i = 0$  the Fano decoder requests the best branch metric, and when  $t_i = 1$  it requests the worst branch metric. To make the ACSU compatible with the irregular tree structure of PAC codes, we use a force-zero (FZ) signal that forces the select module of ACSU to choose  $m_0$ , whenever the Fano decoder is examining a frozen bit. More precisely,  $\text{FZ} = 1$  for  $i \in \mathcal{A}^c$  and  $\text{FZ} = 0$  for  $i \in \mathcal{A}$ . The outputs of ACSU are the path metric of forward node  $\Gamma_i$  and the estimated value of convolution input  $\hat{v}_i$ .

3) *Fano Decoder*: To implement the Fano algorithm, we modify the design introduced in [26] to be compatible with the PAC codes. Fig. 8 shows the block diagram of the PAC Fano decoder. It mainly comprises a polar demapper (PD), a metric calculator, a Fano algorithm control unit, three counters, two registers for storing the convolution input (V-REG) and output (U-REG), a path metric history unit (Metric RAM), and a convolutional encoder (CONV). The Fano algorithm control unit generates control signals to activate the polar demapper and the metric calculator blocks and provides the required inputs for the operation of these blocks.

To extract  $z_i$  from  $\mathbf{z}$  (the output of polar demapper), an  $N$ -to-1 multiplexer of width  $Q$  has been used. V-REG is a

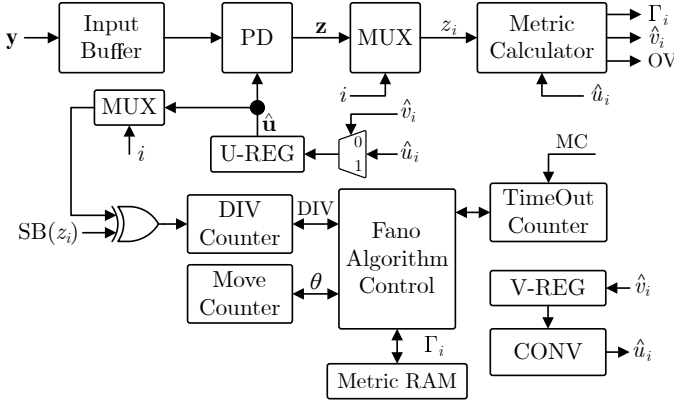


Fig. 8. PAC Fano decoder.

bidirectional shift register used to store the convolution input estimates  $\hat{\mathbf{v}}$ . Whenever the Fano decoder moves forward, the convolution input estimate  $\hat{v}_i$  that has been generated by the metric calculator is stored in V-REG. To avoid any possible data loss during the backtracking of the Fano decoder, the size of V-REG is chosen to be  $N+h$ , where  $h$  is the memory size of the convolution. A convolution block (CONV) uses the data of V-REG to generate the convolution outputs  $\hat{u}_i = (\hat{u}_{i,0}, \hat{u}_{i,1})$ . CONV is a replica of the convolution block used inside the PAC encoder, and it shares the same generator polynomial  $c$ . The U-REG register is used to store the prior convolution output estimates  $\hat{\mathbf{u}}$ . When the Fano decoder moves forward, depending on the branch it chooses, either  $\hat{u}_{i,0}$  or  $\hat{u}_{i,1}$  is stored in the U-REG. A random-access memory (RAM) block is used for storing the path metric vector  $\Gamma = (\Gamma_1, \Gamma_2, \dots, \Gamma_N)$  for the path being explored by the Fano decoder.

The Fano algorithm control unit is a finite-state machine (FSM) that carries out the timing schedule by activating the corresponding blocks and providing their necessary inputs. The state diagram of this unit is shown in Fig. 9. The labels  $S_0$  to  $S_7$  represent the states of the Fano decoder. The state transitions happen according to the control signals  $C_0$  to  $C_7$  and OV (output valid) output signal of the metric calculator block. In this figure, !C denotes the logical complement of C, and the & and | operators represent the logical AND and OR operations, respectively. The state names corresponding to  $S_0$  to  $S_7$  and expressions for generating the state transition signals  $C_1$  to  $C_7$  are listed in Table II. The vector  $\mathcal{A}$  indicates the frozen bits indices such that  $A_i = 0$  if  $i \in \mathcal{A}^c$ , and  $A_i = 1$  if  $i \in \mathcal{A}$ .

To employ the tree search constraints discussed in Section III, we use two counters: DIV Counter and Move Counter. DIV counter is a bidirectional counter which is enabled by the output of the XOR gate that compares the SC path and Fano path. Consequently, this counter is only enabled if the SC path diverges from the Fano path. The counting direction (up/down) of the DIV counter is determined by the Fano decoder such that it counts up or down whenever the Fano decoder moves forward or backward, respectively. On the other hand, the move counter is an up counter which increments every time the Fano decoder moves either forward or backward. Additionally, for practical implementation, a strict limit on the number of

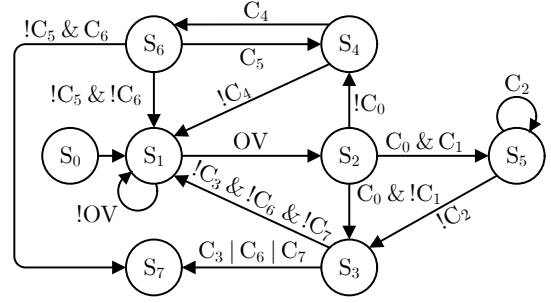


Fig. 9. Fano algorithm control unit state diagram.

clock cycles per decoding session is set by MC. The decoding of a codeword is terminated whenever the number of clock cycles for that session exceeds MC.

TABLE II  
STATES AND STATE TRANSITION SIGNALS OF FANO ALGORITHM CONTROL UNIT.

Label	State	Signal	Expression
$S_0$	initialize	$C_0$	$\Gamma_i \geq T$
$S_1$	request metric	$C_1$	$\Gamma_{i-1} < T + \Delta$
$S_2$	look forward	$C_2$	$\Gamma_i \geq T + \Delta$
$S_3$	move forward	$C_3$	$i = N$
$S_4$	look back	$C_4$	$\Gamma_{i-2} \geq T$
$S_5$	tighten threshold	$C_5$	$t_i = 1$ OR $i \in \mathcal{A}^c$
$S_6$	move back	$C_6$	$\theta > \theta_{\max}$
$S_7$	stop	$C_7$	$\text{DIV} > \text{DIV}_{\max}$

## V. PERFORMANCE RESULTS

In this section, the implementation result of the proposed PAC Fano decoder is presented. The architecture is implemented both on FPGA and ASIC for block lengths of  $N = 128$  and message length of  $K = 64$ . With FPGA implementation, we investigate the FER performance of the decoder and study the number of lookup tables (LUTs), and flip-flops (FFs) used. We also calculate the average number of clock cycles required to decode a single codeword for a given SNR, which will be used to estimate the average information throughput of the PAC decoder. With ASIC implementation, we study the area and power consumption as well as the maximum clock frequency at which the decoder can be clocked.

In both FPGA and ASIC implementations, we use  $\Delta = 2$ ,  $Q = 7$ . We chose the data set index  $\mathcal{A}$  according to the Reed-Muller (RM) scoring rule as explained in [1]. All the PAC Fano decoders are optimised to perform at  $E_b/N_0 = 3.5$  dB, i.e. the channel LLRs of (1) are calculated using a noise variance corresponding to  $E_b/N_0 = 3.5$  dB. To avoid any overflow we set the column width of metric RAM to  $1 + \lceil \log(N \times 2^{Qm-1}) \rceil = n + Q = 14$  bits.

### A. FPGA Implementation Results

The proposed architecture for the PAC Fano decoder is tested on Xilinx Nexys 4 Artix<sup>®</sup>-7 (28 nm) FPGA at 100MHz clock frequency. Table III shows the place-and-route results of the proposed PAC Fano decoder on the FPGA for a block length of 128 and code rate of 1/2.

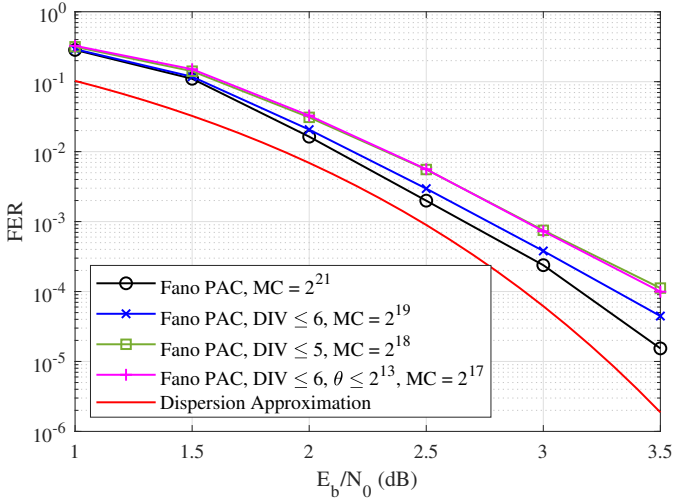


Fig. 10. FER performance of PAC Fano decoder for  $N = 128$ .

TABLE III  
FPGA RESOURCE UTILIZATION

N	K	LUT	FF	RAM (bits)
128	64	16153	8412	1792

To evaluate the error-correction performance and measure the search complexity of the PAC Fano decoder, we used the test setup of Fig. 12. Pseudorandom messages are generated and encoded using MATLAB<sup>®</sup> software. The codeword is modulated using a binary phase-shift keying (BPSK) modulator. White Gaussian noise with a variance corresponding to the test SNR point is added to the BPSK signal. The noisy signal is transmitted to the FPGA through the serial port. Finally, the decoded message is received and compared with the actual transmitted message. Also transmitted by the FPGA is the number of clock cycles spent to decode the current codeword (not shown in the figure).

Fig. 10 plots the FER performance of the decoder for block length of  $N = 128$  under no/different search constraints. Also shown in this figure is the dispersion approximation. The maximum allowed clock cycle per codeword (MC) changes depending on the search limiting technique. These MC values are obtained by simulations to minimize the FER performance degradation. Under no search constraints the decoder can reach  $\text{FER} = 10^{-5}$  at  $E_b/N_0 \approx 3.6$  dB. From this figure, we can see that as we increase the value of maximum number of diversions  $\text{DIV}_{\max}$ , the FER performance of the decoder improves. For a fixed value of  $\text{DIV}_{\max}$  adding a number of moves constraint  $\theta_{\max}$  degrades the FER performance of PAC Fano decoder further. In fact the PAC Fano decoder with  $\text{DIV}_{\max} = 6$  and  $\theta_{\max} = 2^{13}$  constraints has a FER performance very close to the FER performance of a PAC Fano decoder with  $\text{DIV}_{\max} = 5$  constraint.

Fig. 11 shows the average number of clock cycles required by the decoder for decoding a single codeword under no/different search constraints. As expected, since the search complexity of the Fano decoder is highly dependant on the severity of noise, the average number of clock cycles per

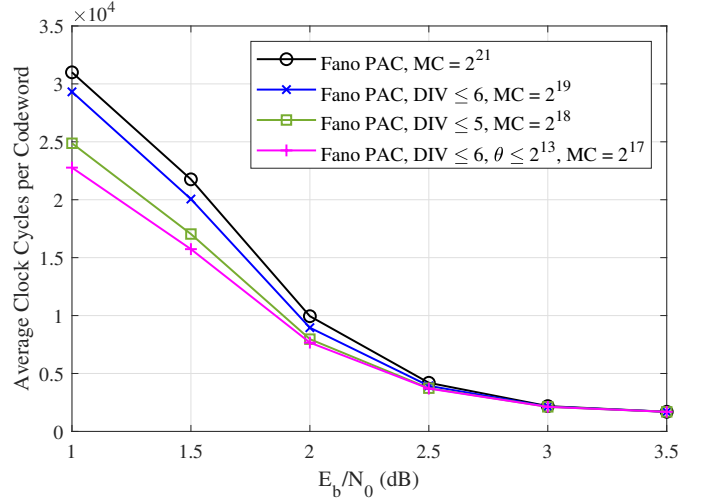


Fig. 11. Average number of clock cycles required for decoding one codeword.

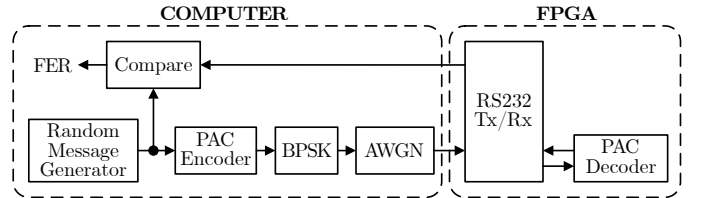


Fig. 12. FPGA test setup of proposed PAC Fano decoder.

codeword decreases as the SNR increases. Depending on the search limiting techniques, the average number of clock cycles per codeword drops by 5% to 26% at  $E_b/N_0 = 1$  dB. The complexity gap between the constrained and unconstrained decoder vanishes at high SNR regime. Larger values of  $\text{DIV}_{\max}$  allow the Fano decoder to explore more branches of the code tree, which results in a better FER performance but spending more clock cycles for decoding a codeword. From the comparisons in Fig. 10 and Fig. 11 we can see that combining the maximum number of moves constraint with the maximum number of diversions constraint is more effective than using the maximum number of diversions constraint only. While maintaining same FER performance, the search complexity of Fano decoder under  $\text{DIV}_{\max} = 6$  and  $\theta_{\max} = 2^{13}$  constraints is lower than the search complexity of the Fano decoder under  $\text{DIV}_{\max} = 5$  constraint. Combining  $\text{DIV}_{\max} = 6$  and  $\theta_{\max} = 2^{13}$  reduces the average number of clock cycles per codeword by 26% at  $E_b/N_0 = 1$  dB.

## B. Post-Synthesis Results

Table IV lists the post-synthesis results of the proposed PAC Fano decoder using Cadence<sup>®</sup> Innovus<sup>™</sup> Implementation System for a block lengths of 128 with TSMC 28 nm 0.72 V library. We present the results for unconstrained decoder with  $\text{MC} = 2^{21}$  and constrained decoder of Fig. 10 with  $\text{DIV}_{\max} = 6$ ,  $\theta_{\max} = 2^{13}$ , and  $\text{MC} = 2^{17}$ .

The decoder occupies an area of 0.065 mm<sup>2</sup> and is capable of operating at 400 MHz consuming 3.63 mW power. The power value is estimated with Cadence<sup>®</sup> Innovus<sup>™</sup> IC Power

Integrity Solution using  $10^4$  pseudorandom input vectors. To estimate the average information throughput (TP) of the proposed PAC Fano decoder, we use the average number of clock cycles required to decode a codeword, which can be obtained from Fig. 11, and the following relationship

$$\text{TP [bit/s]} = \frac{\text{Clock Frequency [cycle/s]}}{\text{Average Cycle [cycle/bit]}} \times K.$$

The performance values for both constrained and unconstrained PAC Fano decoders are reported at  $E_b/N_0 = 3.5$  dB, and the average values are calculated from  $10^7$  decoding trials. As expected from Fig. 11 tree search constraining technique does not improve the average throughput, but it improves the worst-case (W.-C.) throughput and worst-case latency by a factor of 16. The proposed PAC Fano decoder reaches an average information throughput of 15 Mb/s with an average latency of 1,694 clock cycles (CCs) or 4.2  $\mu\text{s}$ .

TABLE IV  
ASIC IMPLEMENTATION RESULTS

Technology	28 nm	
N	128	
K	64	
Supply Voltage (V)	0.72	
Frequency (MHz)	400	
Area (mm <sup>2</sup> )	0.065	
Power (mW)	3.63	
	unconst. <sup>a</sup>	const. <sup>b</sup>
Avg. Info. TP <sup>†</sup> (Mb/s)	15.10	15.16
W.-C. Info. TP* (Mb/s)	0.012	0.195
Avg. Latency <sup>†</sup> ( $\mu\text{s}$ )	4.24	4.22
Avg. Latency <sup>†</sup> (CCs)	1694.87	1689.06
W.-C. Latency (ms)	5.24	0.33
W.-C. Latency (CCs)	$2^{21}$	$2^{17}$
Area Efficiency <sup>†</sup> (Mb/s/mm <sup>2</sup> )	232	233
Power Density (W/mm <sup>2</sup> )	0.056	0.056
Energy Efficiency <sup>†</sup> (PJ/bit)	240.0	239.2

<sup>a</sup>Decoder with no search constraints and  $\text{MC} = 2^{21}$ .

<sup>b</sup>Constrained decoder with  $\text{DIV}_{\text{max}} = 6$ ,  $\theta_{\text{max}} = 2^{13}$ , and  $\text{MC} = 2^{17}$ .

<sup>†</sup>Average value at  $E_b/N_0 = 3.5$  dB, calculated from  $10^7$  decoding trials.

### C. Comparison with Polar Codes Decoders

We compare the unconstrained PAC Fano decoder of Fig. 10 against five different decoders for polar codes with block lengths of  $N = 128$  and  $N = 1024$ . Kestel *et al.* [11] present high throughput SC decoder for (128, 64) polar codes, SCL decoder with a list size of 8 and CRC length of 6 for (128, 70) polar codes, and SCL decoder with a list size of 2 for (1024, 512) polar codes, all fabricated in 28 nm CMOS FD-SOI technology. Giard *et al.* [14] present a flexible SCL decoder with a list size of 4 for (1024, 512) polar codes fabricated in 28 nm CMOS FD-SOI technology. Park *et al.* [15] present a rate-flexible BP decoder for (1024, 512) polar codes fabricated in 65 nm CMOS TSMC technology.

Fig. 13 compares the FER performance of the proposed PAC Fano decoder against decoders of polar codes mentioned above. For the same block length ( $N = 128$ ) PAC codes outperform polar codes. Compared to SC (128, 64) and SCL8-CRC6 (128, 70), PAC Fano decoder has a coding gain of

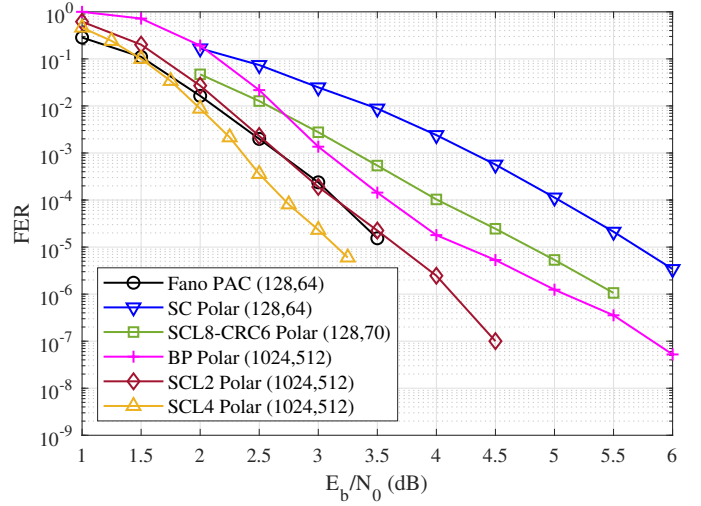


Fig. 13. FER performance comparison of PAC Fano decoder with decoders of Polar codes.

approximately 2.1 dB and 1.2 dB at  $\text{FER} = 10^{-5}$ , respectively. Comparing PAC codes of length 128 with polar codes of length 1024, the proposed PAC Fano decoder performs better than the BP decoder with a coding gain of approximately 0.6 dB at  $\text{FER} = 10^{-5}$ . The PAC Fano decoder performs close to the SCL decoder with a list size of 2 of (1024, 512) polar codes. Using a list size of 4, the SCL decoder of (1024, 512) polar codes outperforms the proposed Fano decoder of (128, 64) PAC codes with a coding gain of 0.4 dB at  $\text{FER} = 10^{-5}$ .

Table V shows a comparison of our PAC Fano decoder against the other ASIC decoders of polar codes. We present PAC Fano decoder results for two different modes: unconstrained decoder and constrained decoder of Fig. 10 with  $\text{DIV}_{\text{max}} = 6$  and  $\theta_{\text{max}} = 2^{13}$ . Since the results of other decoders are for other technologies and supply voltages, for a fair comparison, we provide the normalized results as well. Comparing our PAC Fano decoder with the normalized results of polar decoders, it can be seen from Table V that the PAC Fano decoder has the smallest area (slightly smaller than SC decoder) and power consumption while the SCL2 and SC decoders of [11] have the highest throughput and the best energy efficiency, respectively. It should be noted, however, that the FER performance of the PAC Fano decoder is significantly better than that of the SC decoder. The energy efficiency of the proposed PAC Fano decoder is slightly smaller than the SCL4 decoder of [14].

Benefiting from pipelining and unrolling techniques, SC and SCL decoders of polar codes are capable of achieving high throughput values. However, because of the Fano decoder's backtracking feature, the PAC Fano decoder requires to decode one codeword at a time and hence suffers from low throughput. Among all the decoders, the PAC Fano decoder has the lowest throughput, which is approximately ten times lower than that of the SCL4 decoder of [14] and approximately 17,200 times lower than that of the SCL2 decoder of [11].

TABLE V  
COMPARISON OF THE PAC FANO DECODER AGAINST THE OTHER ASIC DECODERS FOR POLAR CODES.

Implementation	This work		[11]			[14]			[15]	
Algorithm	Fano <sup>a</sup>	Fano Const. <sup>b</sup>	SC	SCL8-CRC6	SCL2	SCL4			BP (15 iter.)	
$(N, K)$	(128,64)	(128,64)	(128,64)	(128,70)	(1024,512)	(1024,512)			(1024,512)	
$E_b/N_0$ at FER = $10^{-5}$	3.6 dB	4.0 dB	5.7 dB	4.8 dB	3.7 dB	3.2 dB			4.2 dB	
Technology	28 nm	28 nm	28 nm	28 nm	28 nm	28 nm			65 nm	
Supply (V)	0.72	0.72	1.0	1.0	1.0	1.3	0.9	0.5	1.0	0.475
Frequency (MHz)	400	400	503	418	503	721	308	20	300	50
Area (mm <sup>2</sup> )	0.065	0.065	0.07	3.15	7.52	0.44			1.48	
Power (mW)	3.6	3.6	80	3340	4530	128.3	23.3	0.6	477.5	18.6
Avg. Coded TP (Mb/s)	30.21 <sup>†</sup>	30.31 <sup>†</sup>	64000	53000	516000	306.8	130.9	8.5	4675.8 <sup>◊</sup>	779.3 <sup>◊</sup>
W.-C. Coded TP (Mb/s)	0.024	0.391	64000	53000	516000	306.8	130.9	8.5	2048	341.3
Avg. Latency ( $\mu$ s)	4.24 <sup>†</sup>	4.22 <sup>†</sup>	0.0179	0.1413	0.292	3.34	7.82	120.4	0.219 <sup>◊</sup>	1.314 <sup>◊</sup>
W.-C. Latency ( $\mu$ s)	5242.88	327.68	0.0179	0.1413	0.292	3.34	7.82	120.4	0.5	3
Area Eff. (Gb/s/mm <sup>2</sup> )	0.465 <sup>†</sup>	0.467 <sup>†</sup>	931	17	69	0.692	0.295	0.019	3.168 <sup>◊</sup>	0.528 <sup>◊</sup>
Energy Eff. (pJ/bit)	120.01 <sup>†</sup>	119.6 <sup>†</sup>	1.28	62.46	8.79	418.3	178.1	64.7	102.1 <sup>◊</sup>	23.8 <sup>◊</sup>
<i>Normalized for 28 nm and 0.72 V</i>										
Frequency (MHz)	400	400	503	418	503	721	–	–	696	–
Area (mm <sup>2</sup> )	0.065	0.065	0.07	3.15	7.52	0.44	–	–	0.277	–
Power (mW)	3.63	3.63	41.47	1731.46	2348.35	39.35	–	–	106.63	–
Avg. Coded TP (Mb/s)	30.21 <sup>†</sup>	30.31 <sup>†</sup>	64000	53000	516000	306.8	–	–	10854.54 <sup>◊</sup>	–
W.-C. Coded TP (Mb/s)	0.024	0.391	64000	53000	516000	306.8	–	–	4754.29	–
Avg. Latency ( $\mu$ s)	4.24 <sup>†</sup>	4.22 <sup>†</sup>	0.0179	0.1413	0.292	3.34	–	–	0.0943 <sup>◊</sup>	–
W.-C. Latency ( $\mu$ s)	5242.88	327.68	0.0179	0.1413	0.292	3.34	–	–	0.2154	–
Area Eff. (Mb/s/mm <sup>2</sup> )	0.465 <sup>†</sup>	0.467 <sup>†</sup>	931	17	69	0.692	–	–	39.632 <sup>◊</sup>	–
Energy Eff. (pJ/bit)	120.01 <sup>†</sup>	119.6 <sup>†</sup>	0.663	32.379	4.557	128.311	–	–	9.821 <sup>◊</sup>	–

<sup>a</sup>Decoder with no search constraints and MC =  $2^{21}$ .

<sup>b</sup>Constrained decoder with  $\text{DIV}_{\max} = 6$ ,  $\theta_{\max} = 2^{13}$ , and MC =  $2^{17}$ .

<sup>†</sup>Average value at  $E_b/N_0 = 3.5$  dB, calculated from  $10^7$  decoding trials.

<sup>◊</sup>Average value at  $E_b/N_0 = 4$  dB with early termination and an average number of iterations of 6.57.

## VI. CONCLUSION

In this paper, we proposed a hardware architecture for decoding PAC codes using the Fano algorithm. Post-synthesis results for 28 nm CMOS TSMC technology showed that the proposed PAC Fano decoder is capable of providing an average information throughput of approximately 15.1 Mb/s at 3.5 dB SNR with a power consumption of 3.63 mW and an area of 0.065 mm<sup>2</sup> for a block length of 128 and code rate  $R = 1/2$ .

Because of their high computational complexity, PAC codes suffer from limited throughput compared to polar codes. At 3.5 dB SNR value, the decoder requires approximately 1,700 clock cycles on average for decoding one codeword for a PAC code of block length 128 and code rate 1/2. We implemented two early termination techniques to maintain a trade-off between the error-correction performance and the decoding complexity by limiting the maximum number of moves of the Fano decoder and the maximum number of diversions between the SC path and Fano path. Simulation results showed that this technique reduces the average computational complexity of the PAC Fano decoder at the cost of marginally sacrificing error-correction performance. This computational complexity reduction becomes significant at lower SNR values.

Even though the throughput is limited because of their extreme error-correction performance, PAC codes could be favorable for cases where reliable communication is more important than throughput. PAC codes use a very simple encoder which concatenates a rate one convolution and a rate one polar transform. Because of this simple structure of encoding and low power decoding, one of the potential use cases of PAC codes could be the Internet of Things (IoT),

for which reliable communication and moderate throughput is of great interest. Also, for the use cases such as control channels where immediate transmission of short-length data is required and packet concatenation is not possible, because of their superior performance, PAC codes could be favorable over polar codes.

Among other things, the number of quantization level plays an important role in the computational complexity of the Fano decoder [36, p. 369]. In this paper, the specified choice for the number of quantization levels for the LLR values ( $Q = 7$ ) was to minimize the area and obtain a reasonable FER performance. The optimization of the computational complexity of sequential decoding of PAC codes subject to the number of quantization levels is yet to be investigated.

## ACKNOWLEDGMENT

The author acknowledges Professor Erdal Arkan for invaluable guidance and support throughout this work. The author is also grateful to the reviewers for their constructive suggestions and comments.

## REFERENCES

- [1] E. Arkan, "From sequential decoding to channel polarization and back again," *arXiv preprint arXiv:1908.09594*, 2019.
- [2] —, "Channel polarization: A method for constructing capacity-achieving codes for symmetric binary-input memoryless channels," *IEEE Transactions on information Theory*, vol. 55, no. 7, pp. 3051–3073, 2009.
- [3] P. Elias, "Coding for noisy channels," *IRE Conv. Rec.*, vol. 3, pp. 37–46, 1955.

- [4] C. Leroux, I. Tal, A. Vardy, and W. J. Gross, "Hardware architectures for successive cancellation decoding of polar codes," in *2011 IEEE International Conference on Acoustics, Speech and Signal Processing (ICASSP)*, 2011, pp. 1665–1668.
- [5] C. Leroux, A. J. Raymond, G. Sarkis, and W. J. Gross, "A semi-parallel successive-cancellation decoder for polar codes," *IEEE Transactions on Signal Processing*, vol. 61, no. 2, pp. 289–299, 2013.
- [6] C. Zhang and K. K. Parhi, "Low-latency sequential and overlapped architectures for successive cancellation polar decoder," *IEEE Transactions on Signal Processing*, vol. 61, no. 10, pp. 2429–2441, 2013.
- [7] C. Leroux, A. J. Raymond, G. Sarkis, I. Tal, A. Vardy, and W. J. Gross, "Hardware implementation of successive-cancellation decoders for polar codes," *Journal of Signal Processing Systems*, vol. 69, no. 3, pp. 305–315, 2012.
- [8] P. Giard, G. Sarkis, C. Thibeault, and W. J. Gross, "237 gbit/s unrolled hardware polar decoder," *Electronics Letters*, vol. 51, no. 10, pp. 762–763, 2015.
- [9] —, "Unrolled polar decoders, part I: hardware architectures," *May*, vol. 6, pp. 1–10, 2015.
- [10] —, "Multi-mode unrolled architectures for polar decoders," *IEEE Transactions on Circuits and Systems I: Regular Papers*, vol. 63, no. 9, pp. 1443–1453, 2016.
- [11] C. Kestel, L. Johannsen, O. Griebel, J. Jimenez, T. Vogt, T. Lehnigk-Emden, and N. Wehn, "A 506 Gbit/s polar successive cancellation list decoder with CRC," in *2020 IEEE 31st Annual International Symposium on Personal, Indoor and Mobile Radio Communications*, 2020, pp. 1–7.
- [12] I. Tal and A. Vardy, "List decoding of polar codes," *IEEE Transactions on Information Theory*, vol. 61, no. 5, pp. 2213–2226, 2015.
- [13] P. Giard, A. Balatsoukas-Stimming, T. C. Müller, A. Burg, C. Thibeault, and W. J. Gross, "A multi-Gbps unrolled hardware list decoder for a systematic polar code," in *2016 50th Asilomar Conference on Signals, Systems and Computers*. IEEE, 2016, pp. 1194–1198.
- [14] P. Giard, A. Balatsoukas-Stimming, T. C. Müller, A. Bonetti, C. Thibeault, W. J. Gross, P. Flatresse, and A. Burg, "Polarbear: A 28-nm FD-SOI ASIC for decoding of polar codes," *IEEE Journal on Emerging and Selected Topics in Circuits and Systems*, vol. 7, no. 4, pp. 616–629, 2017.
- [15] Y. S. Park, Y. Tao, S. Sun, and Z. Zhang, "A 4.68 Gb/s belief propagation polar decoder with bit-splitting register file," in *2014 Symposium on VLSI Circuits Digest of Technical Papers*. IEEE, 2014, pp. 1–2.
- [16] A. Viterbi, "Error bounds for convolutional codes and an asymptotically optimum decoding algorithm," *IEEE transactions on Information Theory*, vol. 13, no. 2, pp. 260–269, 1967.
- [17] L. Bahl, J. Cocke, F. Jelinek, and J. Raviv, "Optimal decoding of linear codes for minimizing symbol error rate (corresp.)," *IEEE Transactions on information theory*, vol. 20, no. 2, pp. 284–287, 1974.
- [18] J. M. Wozencraft, "Sequential decoding for reliable communication," Research Laboratory of Electronics, MIT, Cambridge, Tech. Rep., 1957.
- [19] J. L. Massey, "Threshold decoding," Research Laboratory of Electronics, MIT, Cambridge, Tech. Rep., 1963.
- [20] R. M. Fano, "A heuristic discussion of probabilistic decoding," *IEEE Transactions on Information Theory*, vol. 9, no. 2, pp. 64–74, 1963.
- [21] K. Zigangirov, "Some sequential decoding procedures," *Problemy Peredachi Informatsii*, vol. 2, no. 4, pp. 13–25, 1966.
- [22] F. Jelinek, "Fast sequential decoding algorithm using a stack," *IBM journal of research and development*, vol. 13, no. 6, pp. 675–685, 1969.
- [23] R. Xu, T. Kocak, G. Woodward, K. Morris, and C. Dolwin, "Bidirectional fano algorithm for high throughput sequential decoding," in *2009 IEEE 20th International Symposium on Personal, Indoor and Mobile Radio Communications*. IEEE, 2009, pp. 1809–1813.
- [24] R. Xu, K. Morris, G. Woodward, and T. Kocak, "Low-complexity high-throughput decoding architecture for convolutional codes," *EURASIP Journal on Wireless Communications and Networking*, vol. 2012, no. 1, pp. 1–14, 2012.
- [25] R. Xu, T. Kocak, G. Woodward, K. Morris, and C. Dolwin, "High throughput parallel fano decoding," *IEEE transactions on communications*, vol. 59, no. 9, pp. 2394–2405, 2011.
- [26] M. Benaissa and Y. Zhu, "Reconfigurable hardware architectures for sequential and hybrid decoding," *IEEE Transactions on Circuits and Systems I: Regular Papers*, vol. 54, no. 3, pp. 555–565, 2007.
- [27] I. Jacobs, "Sequential decoding for efficient communication from deep space," *IEEE Transactions on Communication Technology*, vol. 15, no. 4, pp. 492–501, 1967.
- [28] J. Layland and W. Lushbaugh, "A flexible high-speed sequential decoder for deep space channels," *IEEE Transactions on Communication Technology*, vol. 19, no. 5, pp. 813–820, 1971.
- [29] G. Forney and E. Bower, "A high-speed sequential decoder: Prototype design and test," *IEEE Transactions on Communication Technology*, vol. 19, no. 5, pp. 821–835, 1971.
- [30] M. Jeong and S. Hong, "SC-Fano decoding of polar codes," *IEEE Access*, vol. 7, pp. 81 682–81 690, 2019.
- [31] Y. Polyanskiy, H. V. Poor, and S. Verdú, "Channel coding rate in the finite blocklength regime," *IEEE Transactions on Information Theory*, vol. 56, no. 5, pp. 2307–2359, 2010.
- [32] M. Moradi, A. Mozammel, K. Qin, and E. Arkan, "Performance and complexity of sequential decoding of PAC codes," *submitted to IEEE Comm. Letters*, 19 Oct. 2020.
- [33] H. Yao, A. Fazeli, and A. Vardy, "List decoding of Arkan's PAC codes," *arXiv preprint arXiv:2005.13711*, 2020.
- [34] M. Rowshan, A. Burg, and E. Viterbo, "Polarization-adjusted convolutional (PAC) codes: Sequential decoding vs list decoding," *arXiv preprint arXiv:2002.06805*, 2020.
- [35] J. Massey, "Variable-length codes and the Fano metric," *IEEE Transactions on Information Theory*, vol. 18, no. 1, pp. 196–198, 1972.
- [36] A. J. Viterbi and J. K. Omura, *Principles of digital communication and coding*. Courier Corporation, 2013.
- [37] R. G. Gallager, *Information theory and reliable communication*. New York: Wiley, 1968, vol. 2.
- [38] M. Moradi, "On the metric and computation of PAC codes," *arXiv preprint arXiv:2012.05511*, 2020.
- [39] P. Trifonov, "Efficient design and decoding of polar codes," *IEEE Transactions on Communications*, vol. 60, no. 11, pp. 3221–3227, 2012.
- [40] A. Balatsoukas-Stimming, M. B. Parizi, and A. Burg, "LLR-based successive cancellation list decoding of polar codes," *IEEE transactions on signal processing*, vol. 63, no. 19, pp. 5165–5179, 2015.



**Amir Mozammel** (S'20) was born in Tabriz, Iran, in 1988. He received the B.S. and M.S. degrees in electrical and electronics engineering from the Istanbul Sehir University, Istanbul, Turkey, in 2015 and 2017, respectively. He is currently a Ph.D. candidate in the Electrical and Electronics Engineering Department, Bilkent University, Ankara, Turkey.